

Simple Coacervation of Guanidinium-Containing Polymers Induced by Monovalent Salt

Seung-Hwan Oh, Jinhoon Lee, Minhwan Lee, Seulwoo Kim, Won Bo Lee, Dong Woog Lee, and Soo-Hyung Choi*



Cite This: *Macromolecules* 2023, 56, 3989–3999



Read Online

ACCESS |



Metrics & More

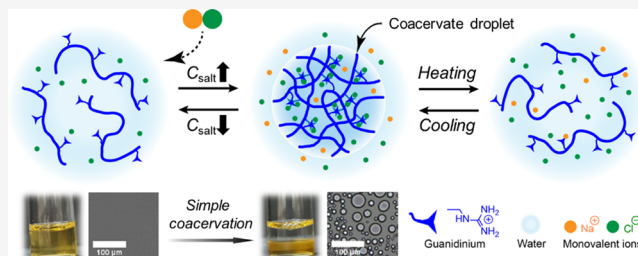


Article Recommendations



Supporting Information

ABSTRACT: Liquid–liquid phase separation (LLPS) of macromolecules, called coacervation, is induced by non-covalent intermolecular associations in aqueous solutions, which is frequently observed in biological processes including cellular compartmentation, signaling, and regulation. Recently, associative interactions between π -conjugated residues have emerged to induce LLPS, along with electrostatic interaction. An arginine residue having a positively charged guanidinium group plays a pivotal role in protein phase behavior because the orientational amphiphilicity of guanidinium groups allows face-to-face π – π stacking despite Coulombic repulsion. In this study, we investigate the simple coacervates of guanidinium-functionalized polyelectrolytes (*i.e.*, poly-arginine) in aqueous media as a function of salt concentration, salt type, and temperature to understand the exclusive role of π -conjugated moieties. Contrary to ammonium-functionalized polyelectrolyte (*i.e.*, poly-lysine) solutions, guanidinium-functionalized polyelectrolyte solutions become turbid by adding monovalent salts and exhibit the upper critical solution temperature (UCST) behavior; the critical temperature is harnessed by salt concentration and salt type. Although a π – π stacked guanidinium pair can exist at a lower salt concentration, LLPS occurs when the number of intermolecular guanidinium pairs goes beyond a critical value to produce the network structure. Furthermore, the enthalpically favored π – π interaction directly affects the bulk rheological behavior and the interfacial property of the coacervates. Our findings provide insights into the underlying interactions of protein phase separation and shed new light on the critical role of π – π stacking in the biological process and material design.



1. INTRODUCTION

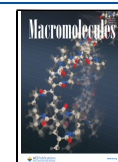
Liquid–liquid phase separation (LLPS) of macromolecules in aqueous media is driven by intra- and intermolecular associations including electrostatic,¹ π – π ,² cation– π ,³ and hydrophobic⁴ interactions, resulting in biphasic liquid mixtures composed of macromolecule-rich coacervates and dilute supernates.^{5,6} The coacervates have a dynamically liquid-like interior, low interfacial tension, and stimuli-responsiveness to external stimuli such as pH, temperature, and ionic strength, and thus, they are useful for a wide range of potential applications including wet adhesives, coating, and food processing.⁷ In recent years, the LLPS of low-complexity intrinsically disordered proteins (IDPs) has been suggested as a primary mechanism to produce membraneless organelles of a liquid-like cellular compartment^{8,9} and underwater adhesion of mussel foot proteins.¹⁰ In addition, numerous neurodegenerative diseases such as Huntington's, Parkinson's, and Alzheimer's diseases are potentially interpreted as abnormal coacervates of misfolded proteins in the human brain.¹¹ Extensive investigation on the coacervates has improved our fundamental understanding of the widespread biological events in organizations, signaling, and regulation.¹²

Over the past decade, the associative π -based interaction has suggested the need to better understand the behavior of biomolecules enriched by π -conjugated moieties.^{2,8} In particular, arginine residues containing a positively charged guanidinium group produce a π – π association with comparable frequency to aromatic groups in a biological context.¹³ Since the guanidinium group is composed of hydrophilic amino edges and hydrophobic planes of conjugated π -orbitals, the spatially orientational amphiphilicity and quasi-aromatic structure enable the guanidinium group to form a face-to-face π – π stacked pair.^{14,15} Coulombic repulsion between the cationic moieties is effectively reduced by counter ions and water molecules, mostly accessible to the partially charged perimeter of the amino edges.^{16,17} Due to the peculiar molecular characteristics, the guanidinium group has been

Received: November 17, 2022

Revised: March 27, 2023

Published: May 15, 2023



studied as a key ingredient of protein denaturant¹⁸ and cell-penetrating peptide.¹⁹ Furthermore, Coulomb-defying guanidinium pairing is responsible for the translocation mechanism across the cellular membrane and is an emerging mechanism to understand the self-aggregation of the arginine-rich polypeptide in aqueous media.^{20,21}

However, much less is known about the coacervation induced by π – π interaction in aqueous media because reliable experimental evidence has been rarely documented. Polyelectrolytes containing the guanidinium group have been employed to induce highly stable polyelectrolyte complexes, but this is mainly attributable to strong affinity to anions by electrostatic attraction and bidentate hydrogen bonding.^{22–24} Recently, the phase separation of the guanidinium-containing polyelectrolytes in aqueous media, called simple coacervation, has been reported and the π – π interaction was proposed to account for the LLPS. Chan-Seng *et al.* reported that comb-like polymers containing guanidinium groups produce a turbid solution in aqueous media without added salts, and the polymers become completely soluble by adding a small amount of NaCl salts.²⁵ However, our group and Tirrell's group reported that guanidinium-functionalized polyelectrolytes are soluble in aqueous media and exhibit phase separation with increasing NaCl concentration.^{26,27} In a biological context, a protamine, as a representative arginine-rich protein, was investigated to show simple coacervation when monovalent and multivalent anions are added, and the coacervates follow upper critical solution temperature (UCST) behavior in aqueous media.^{22–24} Although these works have provided important insights on key information regarding π – π interaction-induced coacervation,^{28,29} the phase separation mechanism considering the effect of salts has not yet been established.^{23,24} This lack of fundamental information about the stability and the function of guanidinium-containing polyelectrolytes and proteins has led to uncertainty about the applications and scientific implications.

In this study, we investigated the simple coacervation of guanidinium-containing polyelectrolytes to quantify the effects of salt and temperature on the phase behavior. The model polyelectrolytes were prepared using guanylation of ammonium-functionalized polyethers, which enables the regulation of LLPS exclusively by switching the cationic charged groups. The monovalent salt concentration-dependent UCST behavior of the polyelectrolyte solutions was clearly observed, and the critical temperature was managed by anion type. The π – π stacking of guanidinium groups was detected by Fourier-transform infrared spectroscopy and molecular dynamics simulation. Furthermore, the role of the π – π interaction for polymer dynamics was quantified by rheology and surface force apparatus measurements. Our findings provide crucial insights into the underlying interactions of protein phase separation and shed new light on the critical role of π – π stacked guanidinium pairs in the biological process and material design.

2. EXPERIMENTAL SECTION

2.1. Polyelectrolyte Synthesis. Guanidinium- or ammonium-functionalized polyelectrolytes were prepared by anionic ring-opening polymerization of poly(allyl glycidyl ether) (PAGE), followed by post-polymerization modification to introduce the charged moieties to the allyl groups, as shown in Scheme S1.^{30–32} Allyl glycidyl ether (AGE, TCI) was degassed by several cycles of the freeze–pump–thaw process, followed by purification with butyl magnesium chloride for 3 h. Tetrahydrofuran (THF), a solvent, was collected from a dry solvent system (Korea Kiyon, Korea) and further purified by *sec*-butyl

lithium for 3 h. Potassium naphthalenide was prepared by mixing potassium metal and naphthalene in dry THF for at least 24 h. Benzyl alcohol (TCI), an initiator, was degassed by several cycles of the freeze–pump–thaw process and injected into a reactor filled with dry THF under an argon condition. Polymerization was initiated by adding potassium naphthalenide solution dropwise until a pale green color appeared. Then, AGE monomers were added and polymerized at 40 °C for 24 h. Anhydrous methanol was added to quench the polymerization, and PAGE was recovered by precipitation in *n*-hexane.

The ammonium functional groups were introduced to PAGE homopolymers by a thiol-ene click reaction.³¹ PAGE and 2,2-dimethoxy-2-phenylacetophenone (DMPA, 0.05 equiv per allyl group), a photo-initiator, were dissolved in methanol, and 2-aminoethanethiol hydrochloride (4 equiv per allyl group, TCI), a functional thiol agent, was dissolved in deionized water. The mixture of the two solutions was purged by argon for 30 min, followed by exposure to UV light under stirring for at least 3 h. Then, the residual reagents were removed by dialysis using a regenerated cellulose tubular membrane (MWCO, 6k–8k; MFPI) in deionized water at pH = 5 for 3 days. Ammonium-functionalized PAGE (A-PAGE) was recovered by lyophilization. Guanidinium-functionalized PAGE (G-PAGE) was obtained by guanylation of A-PAGE using 1H-pyrazole-1-carboxamide hydrochloride (TCI) in a NaOH aqueous solution (ca. pH ~ 10) for a week.³² After the substitution reaction, G-PAGE was recovered by dialysis and lyophilization.

Polymers were characterized by size exclusion chromatography (SEC, JASCO) and ¹H nuclear magnetic resonance spectroscopy (¹H NMR, Unity-Inova 500). SEC traces provided the polydispersity index ($\bar{D} = M_w/M_n$) of PAGE polymers (Figure S1). ¹H NMR was used to estimate the number of the average degrees of polymerization (N_n) of PAGE and the complete conversion of the post-polymerization modification for A-PAGE and G-PAGE (Figure S2). All polymer characteristics are summarized in Table 1.

Table 1. Polymer Characteristics

polymer	N_n	M_n (kg/mol)	\bar{D}
PAGE	100	11.4	1.08
A-PAGE	100	22.8	
G-PAGE	100	27.0	

2.2. Optical Microscopy. Optical microscopy (Olympus BX51) was used to directly visualize the simple coacervates at a microscale. Polyelectrolyte solutions were loaded between two CaF₂ windows with a PTFE spacer of 15 μ m in thickness and annealed at target temperatures for at least 5 min before taking images. The temperature was carefully controlled at the temperature-controlled stage (FTIR SP600, Linkam Scientific).

2.3. Transmittance Measurement. A UV–visible spectrophotometer (8453, Agilent Technologies) was employed to measure the transmittance measurement at a wavelength of 600 nm under stirring (~1200 rpm). Polyelectrolyte solutions were loaded in an optical glass cell, and the temperature was manually controlled by a Peltier temperature controller (TC 1, Quantum Northwest). In addition, a UV–visible spectrophotometer (Cary Bio 100, Agilent Technologies) was used for the temperature-ramping measurement using an automatic temperature controller with a ramping rate of 1 °C/min.

2.4. Fourier-Transfer Infrared Spectroscopy. The Fourier-transfer infrared (FTIR) spectra were obtained by a Nicolet 6700 (Thermo Fisher Scientific) equipped with a deuterated triglycine sulfate (DTGS) detector. The attenuated total reflectance FTIR (ATR-FTIR) spectra were recorded using a ZnSe crystal prism at room temperature. The temperature-dependent FTIR spectra were obtained using the temperature-controlled vertical stage (FTIR SP600, Linkam Scientific) with 0.1 °C accuracy. Samples were loaded between two CaF₂ windows with a PTFE spacer with a thickness of 15 μ m, and the temperature was manually controlled between 0 and

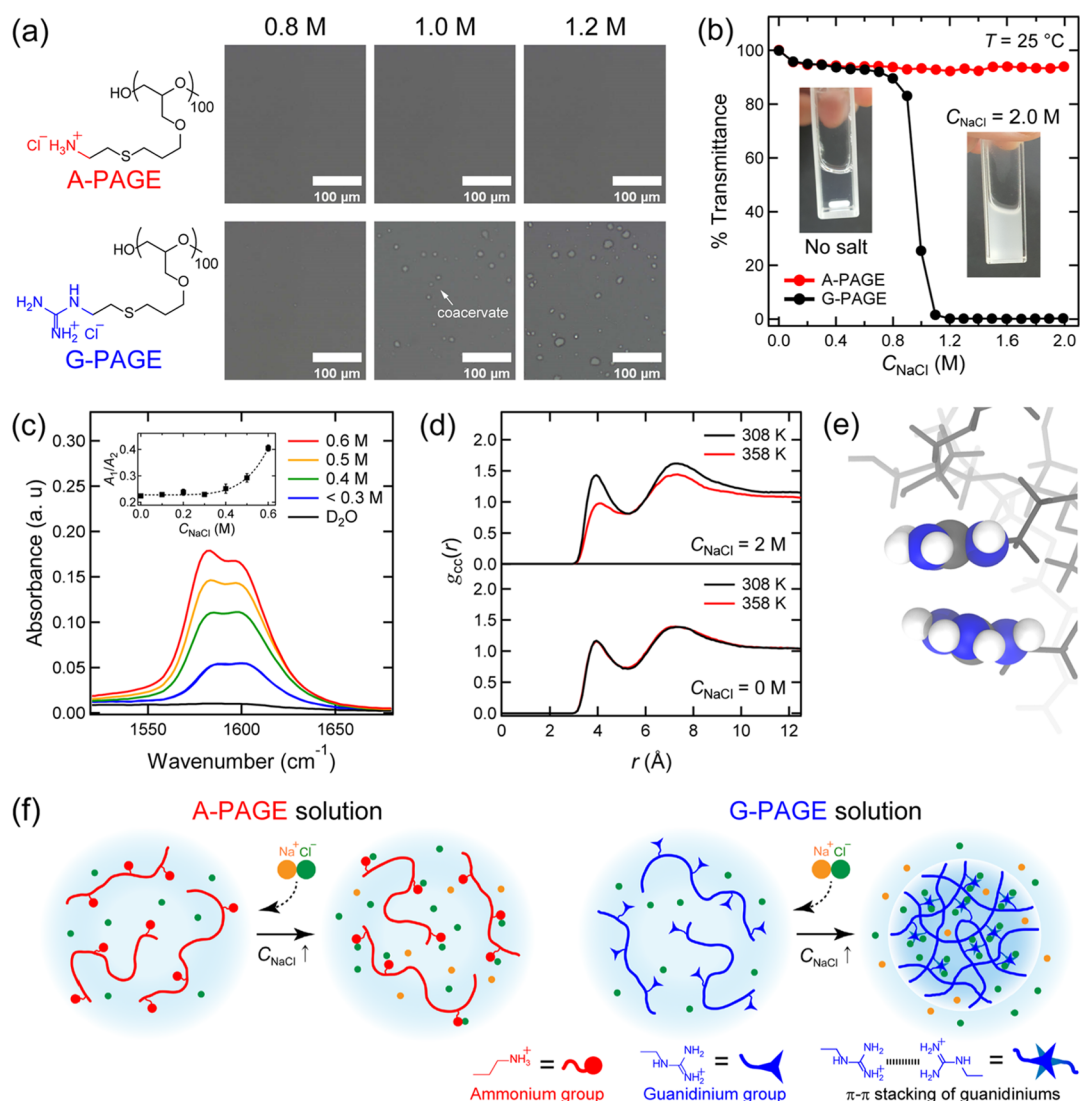


Figure 1. (a) Optical microscopy images of 0.1 wt % A-PAGE (upper) and G-PAGE (lower) solutions at $C_{\text{NaCl}} = 0.8, 1.0, \text{ and } 1.2 \text{ M}$ measured at $25 \text{ }^\circ\text{C}$. The scale bar denotes $100 \mu\text{m}$. The chemical structures of A-PAGE and G-PAGE are represented on the left side. (b) Transmittance obtained from 0.1 wt % A-PAGE solution (red) and G-PAGE solution (black) as a function of C_{NaCl} at $25 \text{ }^\circ\text{C}$. The insets are photos of G-PAGE solutions at $C_{\text{NaCl}} = 0$ and 2.0 M . (c) ATR-FTIR spectra of the CN_3 stretching of guanidinium groups (i.e., $1500\text{--}1700 \text{ cm}^{-1}$)^{51,52} for 20 wt % G-PAGE solutions in D_2O as a function of C_{NaCl} at room temperature. The inset shows the peak areal ratio of A_1 and A_2 as a function of C_{NaCl} , where the guanidinium bands were deconvoluted by two Voigt curves. The dashed line is a guide to the eye. (d) Radial distribution function, $g_{\text{cc}}(r)$, at $C_{\text{NaCl}} = 0$ (bottom) and 2.0 M (top) and at 308 K (black) and 358 K (red). The first peak near 4 \AA indicates the $\pi\text{--}\pi$ stacking distance of the guanidinium groups. (e) Snapshots of the stacked guanidinium dimers are obtained from the MD simulation trajectory. The gray rods represent the polymer backbone, and the background includes sodium and chloride ions and water molecules. (f) Graphical illustration of the A-PAGE and G-PAGE solutions associated with salt addition.

$30 \text{ }^\circ\text{C}$. The FTIR absorbance spectra were collected in the $1000\text{--}4000 \text{ cm}^{-1}$ region, and the solvent background was subtracted.

2.5. Rheological Measurement. The shear rate-dependent viscosity was measured by a rheometer (MCR 302, Anton Paar) equipped with a parallel plate with 25 mm diameter. The temperature was controlled between 1 and $25 \text{ }^\circ\text{C}$ by a Peltier accessory. The coacervate layers of 20 wt % G-PAGE solutions at a target C_{NaCl} were carefully extracted after centrifugation and loaded onto the Peltier plate. Water evaporation was minimized using a homemade acrylic cover.

2.6. All-Atomistic Molecular Dynamics Simulation. The nanoscopic structure of G-PAGE simple coacervates was examined using full atomistic molecular dynamics simulations. All simulations were conducted with the Groming machine for chemical simulations (GROMACS) package,^{33–35} and all-atom optimized potentials for the liquid simulation (OPLS-AA) force field were used to describe the

atomistic interactions. The experimental parameters were obtained from the GROMACS table or LigParGen server.^{36,37} In the simulation box, 10G-PAGE polymer chains containing 30 repeating units, a target number of Na and Cl ions, and 10,500 water molecules were randomly distributed, and then the system energy was minimized. To achieve the equilibrium structure, isothermal–isobaric simulation (i.e., NPT ensemble) was conducted with a velocity-rescaling thermostat and a Berendsen barostat for 10 ns .^{38–40} Then, NPT simulation was performed for 200 ns using a Nosé–Hoover thermostat and the Parrinello–Rahman pressure coupling method.^{41–46} Structure analysis for the guanidinium groups was based on the simulation trajectory for the last 1 ns . The linear constraint solver (LINCS) was applied to neglect the small vibration of the hydrogen atoms, and the long-range electrostatic interaction was treated with the particle mesh Ewald method.⁴⁰

2.7. Miniature Surface Force Apparatus. A miniature surface force apparatus (μ SFA, SurForce LLC, USA) was used to evaluate the interaction energy and the absolute distances between the two polyelectrolyte-coated surfaces.^{47,48} The measurements were performed using a symmetric system for A-PAGE and G-PAGE polyelectrolytes. The polyelectrolyte solutions were prepared by dissolving the polyelectrolytes in deionized water with 0.5 and 1 μ g/mL for A-PAGE and G-PAGE, respectively, followed by filtration using a 0.2 μ m polytetrafluoroethylene filter (ADVANTEC) to exclude aggregates and impurities. As a substrate, a freshly cleaved back-silvered (\sim 50 nm) muscovite mica (Grade #1, S&J Trading, USA) was glued onto a cylindrical disc of 2 cm in radius using an optical adhesive (NOA 81, Norland Products Inc., USA) after UV curing (ca. 50 min).⁴⁷ Then, the polyelectrolyte solutions were drop-casted on the mica surface and then washed with deionized water to remove the unbound molecules. The polyelectrolyte-coated surfaces were aligned in the μ SFA chamber with crossed cylindrical geometry, and \sim 100 μ L of NaCl solution was injected between the two opposing surfaces. The force–distance curves were measured as a function of C_{NaCl} = 0, 0.3, 0.6, 0.9, and 1.2 M for both A-PAGE and G-PAGE polyelectrolytes. To minimize evaporation during the SFA measurements, the chamber was sealed with 2 mL of deionized water and then the surfaces were equilibrated for 1 h.

The force measurements were performed by approaching and retracting the two opposing surfaces with a fine motor at a constant speed of 5 nm/s. In this study, a contact time of 5 s was maintained before retraction. The interaction force (F) was explored by deflecting a double-cantilevered spring ($k = 432.54$ N/m) supporting a lower surface. The absolute mica-to-mica distance was verified through the fringes of equal chromatic order (FECO) based on multiple-beam interferometry (MBI) using a white light beam.⁴⁹ Based on the Johnson–Kendall–Roberts model, the minimum F/R value, the cohesion force between the two surfaces during separation, was converted to cohesion energy per unit area ($W_{\text{co}} = 2F/3\pi R$).^{47,50} All experiments were operated at room temperature ($T = 22.5$ °C) and repeated three times for reproducibility.

2.8. Atomic Force Microscopy (AFM). Atomic force microscopy (AFM, Multimode V AFM, Veeco, USA) was employed to investigate the topography of the polyelectrolyte surfaces under the standard tapping mode in the air using a silicon cantilevered tip (PR-T300, Probes, Korea). The standard sharp tip was attached to the end of the cantilever spring, and spring deflection was reflected on the position-sensitive detector when the tip was close to a surface. The roughness profile was determined using NanoScope Analysis software (Bruker Corporation).

3. RESULTS AND DISCUSSION

3.1. Monovalent Salt-Induced LLPS. Poly(allyl glycidyl ether) (PAGE with $N = 100$ and $D = 1.08$) polymers were synthesized using anionic ring-opening polymerization and functionalized for cationic ammonium (A) or guanidinium (G) groups with chloride counterions, labeled A-PAGE (*i.e.*, polylysine) and G-PAGE (*i.e.*, poly-arginine), respectively (Figure 1a and Scheme S1).²⁶ The number and position of charged groups and the backbone chemical structure for A-PAGE and G-PAGE are identical except for the charge type. The polyelectrolytes were dissolved in deionized water, and NaCl salts were added to adjust the extrinsic salt concentration, C_{NaCl} . It is noted that the intrinsic concentrations of Cl^- counterions released from the polyelectrolytes are 0.004 and 0.8 M for 0.1 and 20 wt % polymer solutions, respectively.

As shown in Figure 1a, the optical microscopy (OM) image highlights that micrometer-sized liquid droplets were formed in 0.1 wt % G-PAGE solutions as C_{NaCl} increases, but droplet formation was not observed in 0.1 wt % A-PAGE solutions regardless of C_{NaCl} . In addition, the transmittance obtained from 0.1 wt % G-PAGE solutions at 25 °C drops sharply near

$C_{\text{NaCl}} = 1.0$ M with increasing C_{NaCl} (Figure 1b). Both observations clearly indicate that the liquid–liquid phase separation (LLPS) of G-PAGE solutions (*i.e.*, simple coacervation) occurs at a higher C_{NaCl} , which is induced by monovalent salts. This C_{NaCl} dependence is apparently in contrast to the behavior of the A-PAGE solution that remains transparent up to the solubility limit of NaCl (Figure S3). Simple coacervation is further evidenced by the 20 wt % G-PAGE solution at $C_{\text{NaCl}} = 1.0$ M, in which viscous polymer-rich coacervates and transparent supernates are produced after centrifugation as macroscopic phase separation (Figure S4). It is noted that the liquid-like simple coacervate of G-PAGE solutions is also triggered by multivalent salts such as sodium sulfate and sodium citrate, while the A-PAGE solutions remain transparent up to the solubility limit of the multivalent salts (Figures S3 and S4). This finding strongly confirms that simple coacervation is exclusively caused by the guanidinium functional groups when Coulombic repulsion is effectively attenuated, and the intermolecular salt bridge between the charged groups is marginal to induce simple coacervation.

Attenuated total reflection Fourier transform infrared (ATR-FTIR) spectroscopy was performed to investigate detailed molecular interactions that are responsible for simple coacervation. Figure 1c displays the representative spectra between 1500 and 1700 cm^{-1} corresponding to the CN_3 stretching of guanidinium groups as a function of C_{NaCl} at room temperature. Since H_2O bending absorption occurs between 1500 and 1700 cm^{-1} , the 20 wt % G-PAGE solutions were prepared in D_2O . The absorption profiles are nearly identical for a C_{NaCl} lower than 0.3 M where the solutions are transparent. However, the intensity is significantly enhanced by increasing the C_{NaCl} above 0.3 M, which indicates that the simple coacervates of G-PAGE solutions begin to form and precipitate on top of the ATR crystal. Since the electrostatic repulsion between guanidinium groups is crucially controlled by the overall anion concentration, lower added C_{NaCl} is required to induce LLPS for 20 wt % G-PAGE solution than 0.1 wt % G-PAGE solution due to released intrinsic counterions.

Since the alkyl substitution at the guanidinium groups results in a broken 3-fold axis of symmetry, the perturbation splits the degeneracy of the guanidyl CN_3 stretching modes by 20 cm^{-1} .^{51,52} The two nearly degenerate normal modes, centered at 1580 and 1600 cm^{-1} , labeled A_1 and A_2 , respectively,⁵³ were adjusted by a sum of two Voigt profiles that is a convolution of Gaussian and Lorentzian distribution⁵⁴ (see Figure S5). The ratio of the integrated areas (*i.e.*, A_1/A_2), corresponding to the transition dipole squared, for the two nearly degenerated components, increases from 0.2 to 0.4 as simple coacervation occurs, as shown in the inset of Figure 1c. Although an unequivocal assignment for the observed peaks is challenging,⁵² this increment reflects that the asymmetric interaction of hydrogen bonding between the NH_2 groups and water molecules becomes gradually enhanced as the simple coacervates are formed, and the distribution of water molecules becomes more uneven around the guanidinium groups.

To provide a detailed molecular picture of the underlying interaction, we performed molecular dynamics (MD) simulations using a system with 10 polymer chains of 30 repeating units, 10,500 H_2O molecules, and a target number of Na^+ and Cl^- ions. Figure 1d displays the radial distribution function, $g_{\text{cc}}(r)$, representing the distance between the centers of mass of the guanidinium groups at $C_{\text{NaCl}} = 0$ and 2 M and at 308 and

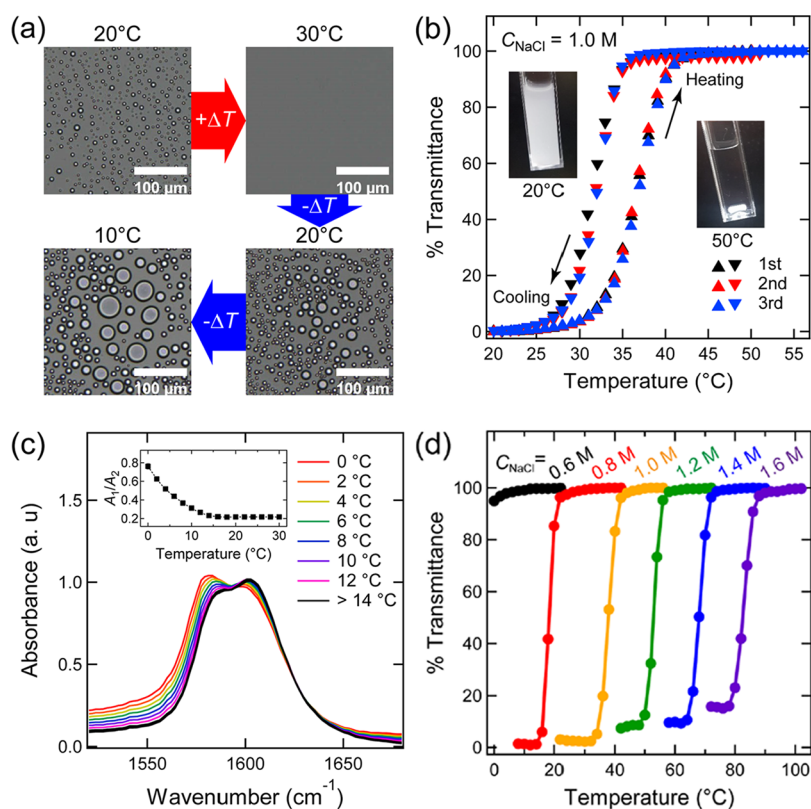


Figure 2. (a) Optical microscopy images obtained from a 10 wt % G-PAGE solution at $C_{\text{NaCl}} = 0.5$ M upon heating and cooling. The scale bar denotes 100 μm . (b) Temperature-dependent transmittance obtained from 0.1 wt % G-PAGE solution at $C_{\text{NaCl}} = 1.0$ M for sequential heating and cooling cycles with a ramping rate of 1 $^{\circ}\text{C}/\text{min}$. Representative photos taken at 20 and 50 $^{\circ}\text{C}$ are shown in the inset. (c) Transmission FTIR spectra of the CN_3 stretching of guanidinium groups for 20 wt % G-PAGE solutions in D_2O as a function of temperature at $C_{\text{NaCl}} = 0.4$ M. The inset shows a peak areal ratio of A_1 and A_2 as a function of temperature. The dashed line is a guide to the eye. (d) Temperature dependence of transmittance for 0.1 wt % G-PAGE solutions at various C_{NaCl} values. The transmittance was measured upon cooling with a cooling rate of 1 $^{\circ}\text{C}/\text{min}$.

358 K. Consistent with previous findings for guanidinium ions using MD and Monte Carlo simulations,^{15,17,20,21,25} the first peak of $g_{\text{cc}}(r)$ observed around 4 \AA is attributed to the staggered fashion of π – π stacked guanidinium pairs, as illustrated in Figure 1e. This like-charge ion-pairing was rationalized by a combination of cavitation effects and quadrupole–quadrupole and dispersion attractions when long-ranged electrostatic repulsion is significantly attenuated in aqueous media.⁵⁵ We observed that the fraction of the π – π stacked guanidinium pair considerably increases with increasing salt concentration at 308 K, deducing that the π – π stacking of the guanidinium groups essentially induces simple coacervation when electrostatic repulsion is effectively screened. In addition, the stacked structure limits ions and water molecules approaching the upper and lower planes of the guanidinium groups, and thus, abundant guanidinium pairing results in the enhanced asymmetric hydrogen bonding of water molecules around the guanidinium groups as observed in the FTIR measurement. The MD simulation also suggests that the guanidinium pairs still exist at a lower C_{NaCl} where simple coacervation does not occur, which is discussed later.

Figure 1f summarizes the salt concentration-dependent behavior of A-PAGE and G-PAGE polyelectrolyte solutions. At low C_{NaCl} , the electrostatic repulsion between cationic groups is dominant to disperse both polyelectrolytes in the aqueous solvent, resulting in a clear solution. Guanidinium groups, however, begin to form the short-ranged π – π stacking

when electrostatic repulsion is effectively screened above a critical salt concentration, which is in contrast to ammonium groups. This physically dynamic interaction results in intermolecular network formation and, thus, macroscopic phase separation of G-PAGE solutions.

3.2. Temperature Dependence. Since the MD simulation showed that the fraction of the stacked guanidinium pairs decreases at higher temperatures (Figure 1d), we investigated the temperature-dependent behavior of the G-PAGE coacervates. OM images confirm that the liquid droplets disappear at high temperatures, followed by nucleation upon cooling (Figure 2a). Figure 2b also shows that the turbid 0.1 wt % G-PAGE solution prepared at $C_{\text{NaCl}} = 1.0$ M becomes transparent as the temperature increases. This temperature dependence is reversible upon sequential heating and cooling cycles, and a kinetic barrier of the nucleation process is evidenced by the observed hysteresis. The upper critical solution temperature (UCST) behavior indicates that the π – π interaction is originated by enthalpy and thus regulated by temperature as well as salt concentration.²⁵ Furthermore, transmission FTIR measurements equipped with a Peltier temperature controller were conducted for 20 wt % G-PAGE solutions at $C_{\text{NaCl}} = 0.4$ M. The absorption spectra corresponding to the CN_3 stretching of the guanidinium group are nearly identical above 14 $^{\circ}\text{C}$ where the solutions are transparent. When the temperature decreases further where coacervation occurs, the peak position, however, shifts

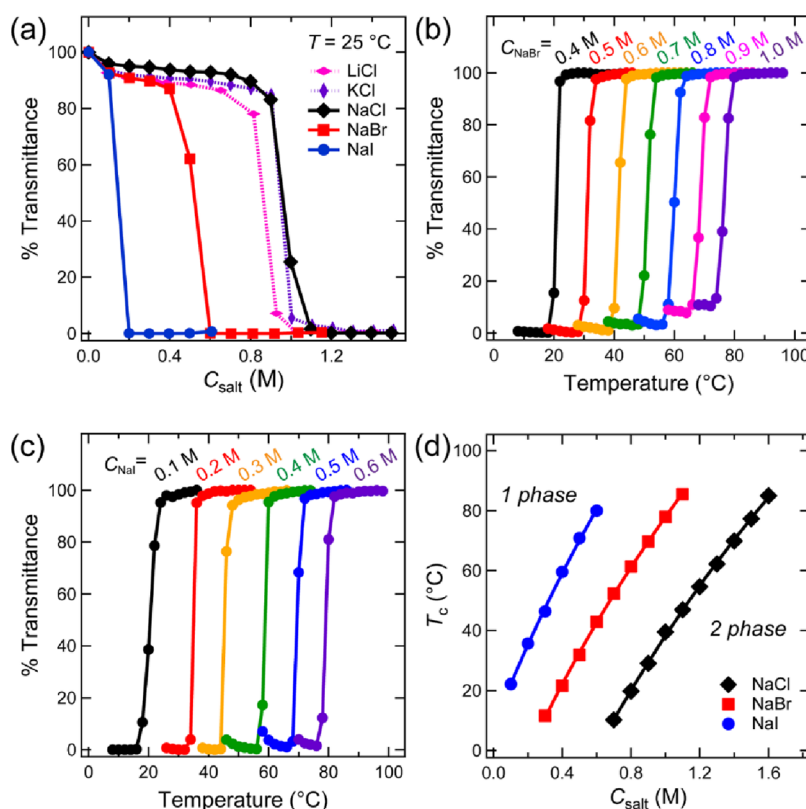


Figure 3. (a) Salt concentration dependence of transmittance for 0.1 wt % G-PAGE solutions as a function of C_{salt} of LiCl (magenta), KCl (purple), NaCl (black), NaBr (red), and NaI (blue) at 25 $^{\circ}\text{C}$. The critical transition temperature, T_c , is nearly independent of the cations such as Li^+ , K^+ , and Na^+ but strongly depends on the anions such as Cl^- , Br^- , and I^- . Temperature dependence of transmittance for 0.1 wt % G-PAGE solutions with (b) NaBr and (c) NaI at various C_{salt} values. (d) Salt concentration-dependent T_c for 0.1 wt % G-PAGE solutions: NaCl (black), NaBr (red), and NaI (blue). The solid line represents the best fit to the Langmuir-type isotherm.

gradually to a lower wavenumber and the areal ratio of A_1 and A_2 (*i.e.*, A_1/A_2) increases from 0.2 to 0.8, as shown in Figure 2c. Consistent with the salt concentration-dependent behavior, the π - π stacked guanidinium pairs become abundant to induce the simple coacervates at a lower temperature.

Figure 2d illustrates the temperature-dependent transmittance of 0.1 wt % G-PAGE solutions at various C_{NaCl} values. A critical transition temperature, T_c , defined as a temperature when the transmittance drops by 80% upon cooling, increases gradually with increasing C_{NaCl} . When the electrostatic repulsion between the guanidinium groups is reduced as C_{NaCl} increases, the probability to form the guanidinium pairs by the π - π interactions becomes higher. Therefore, a larger number of intermolecular guanidinium pairs are created, and higher thermal energy is required to dissociate the coacervates.

3.3. Charge-Type Dependence. The effect of a monovalent charge type on the phase behavior for 0.1 wt % G-PAGE solutions at 25 $^{\circ}\text{C}$ was investigated using LiCl, KCl, NaCl, NaBr, and NaI. We observed that the critical salt concentration is nearly independent of the cation type but strongly depends on the anion type (Figure 3a), indicating that the reduction of the electrostatic repulsion by anions is crucial to produce the π - π stacked structure. Interestingly, the relative effectiveness of the anions apparently follows $\text{I}^- > \text{Br}^- > \text{Cl}^-$, which is the reverse of the Hofmeister prediction in which anions are ordered as $\text{Cl}^- > \text{Br}^- > \text{I}^-$ for better salting-out and, thus, phase separation.⁵⁶ We believe that the higher polarizability and poor hydration energy of larger halogen anions

provide more efficient screening of the electrostatic repulsion between cationic guanidinium groups⁵⁷ (Table S1). Here, T_c for NaI is significantly higher than that for NaCl at the same ionic strength, which underpins that the critical salt concentration and corresponding T_c provide a method to quantify the effectiveness of charge screening of monovalent anions.

Figure 3b,c displays the temperature-dependent transmittance of 0.1 wt % G-PAGE solutions at various C_{salt} values for NaBr and NaI, respectively. Consistent with NaCl, T_c increases gradually with increasing C_{salt} . Remarkably, we observed that the relationship between T_c and C_{salt} of NaI, NaBr, and NaCl is nearly linear, and the saturation behavior was not observed under our experimental conditions (Figure 3d). The pseudo-linear increment of T_c suggests that the number of guanidinium pairs within the coacervates is gradually enhanced with C_{salt} at a certain temperature. Furthermore, since the screening of electrostatic repulsion requires a specific association between anions and guanidinium groups, we propose that the anion association follows the Langmuir-type isotherm and T_c is primarily dominated by the number of π - π stackings as $T_c = aK_A C_{\text{salt}} / (1 + K_A C_{\text{salt}}) + b$, where K_A is an associated equilibrium constant, and a and b are fitting parameters. Cremer and co-workers revealed that the transition temperature for the LLPS of a lysozyme is dependent on the salt concentration and anion type and reported that the anion-specific association is captured by the Langmuir-type isotherm.^{58,59} We observed that the obtained K_A increased from 0.28 to 0.33 in the order of $\text{Cl}^- < \text{Br}^- < \text{I}^-$

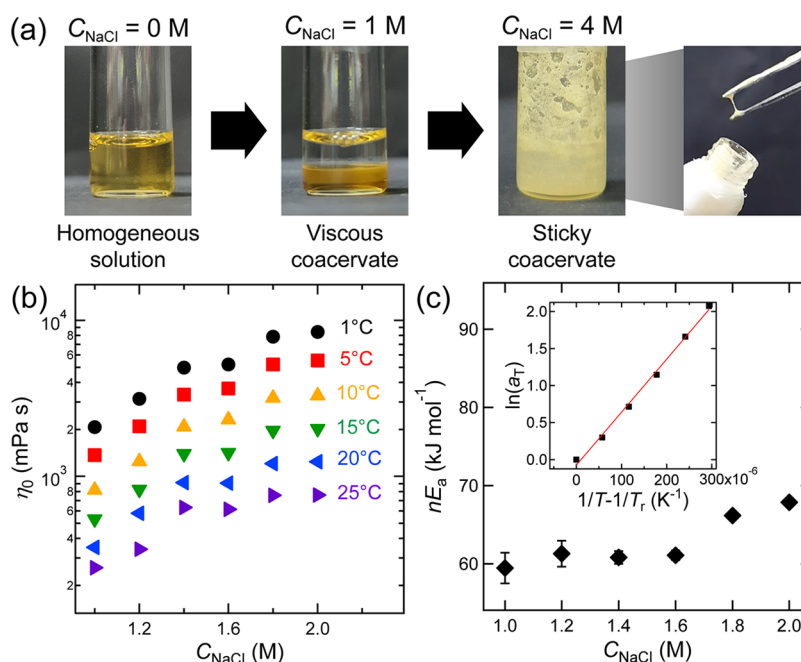


Figure 4. (a) Photographs of 20 wt % G-PAGE solutions at $C_{\text{NaCl}} = 0, 1$, and 4 M. (b) Zero shear viscosity (η_0) of G-PAGE coacervates at various C_{NaCl} values and temperatures. The coacervates were isolated from 20 wt % G-PAGE solutions at target C_{NaCl} . (c) Association energy (nE_a) of the G-PAGE coacervate as a function of C_{NaCl} . The inset represents the temperature-dependent $\ln(a_T)$ for G-PAGE coacervates isolated from a solution at $C_{\text{NaCl}} = 1.0$ M.

(Table S1), which confirms that the larger halogen anions are more effective in associating with the cationic sites and thus in reducing electrostatic repulsion.

3.4. Rheological Measurement. Figure 4a highlights that a liquid-like coacervate prepared by 20 wt % G-PAGE solution becomes sticky mucus with increasing C_{NaCl} up to 4 M, indicating that the chain mobility is highly modulated by the number of guanidinium pairs. To understand the bulk property, the coacervates were isolated by decanting supernates after centrifugation of 20 wt % G-PAGE solutions at room temperature. We obtained the zero-shear viscosity, η_0 , as a function of C_{NaCl} and temperature for the separated coacervates using steady-shear measurements. Figure 4b demonstrates that η_0 increases with increasing C_{NaCl} and/or decreasing temperature (raw data are available in Figure S6). It is noted that the polymer concentration was measured as ~ 45 wt % for the G-PAGE coacervates prepared at $C_{\text{NaCl}} = 1.4$ M using the thermogravimetric method. We reasonably assume that the polymer concentration in the separated coacervates slightly increases with increasing C_{NaCl} , but the difference is marginal within our experimental range.

Recently, the sticky polymer dynamics pioneered by Semenov and Rubinstein have been applied to understand the rheological behavior of complex coacervates, in which the charged groups are considered as stickers to produce a pairwise associative interaction.^{60–63} When associative polymers with the degree of polymerization, N , contain f associating groups separated by neighboring l spacers (*i.e.*, $N = fl$), the unentangled sticky-Rouse model predicts $\eta_0 \sim \tau_b(kT\phi/Nd^3)f^2$, where τ_b , k , T , ϕ , and $1/d^3$ are the lifetime of the associative stickers, Boltzmann constant, absolute temperature, polymer concentration, and chain density, respectively.⁶⁰ For G-PAGE coacervates, larger C_{NaCl} is expected to induce more effective screening of electrostatic repulsion between guanidinium groups, leading to the elevated possibility to form associating

pairs (*i.e.*, larger f). Therefore, the C_{NaCl} -dependent η_0 observed at a fixed temperature is qualitatively consistent with the theoretical prediction, although the salt concentration within the coacervates is not accurately determined.

Also, the shift factor, defined as $a_T = \eta_0/\eta_{0,r}$ where $\eta_{0,r}$ is the zero-shear viscosity at a reference temperature, was computed to account for the temperature-dependent η_0 as shown in the inset of Figure 4c. Here, we assume that the n associating pairs need to break simultaneously to allow relaxation of the polymer chains,^{64,65} and the relaxation time of the associative pairs measured by rheology is given by $\tau_b = \tau_0 \exp(nE_a/kT)$, where τ_0 and E_a are the relaxation times without the associative interaction and the activation energy for dissociation, respectively. Using the shift factor, nE_a at various C_{NaCl} values was estimated with the assumption that the τ_0 is independent of the temperature under our experimental condition. As depicted in Figure 4c, we found that the nE_a slightly increases from 60 to 70 kJ/mol as C_{NaCl} increases from 1.0 to 2.0 M (raw data are available in Figure S7), and thus, the relaxation time increases. This further corroborates the C_{NaCl} dependence of η_0 . Since the interaction energy of guanidinium pairs as a function of ionic strength has not been fully established yet,^{66,67} our observation suggests that both/either the required number of guanidinium groups for the relaxation and/or the interaction energy of guanidinium pair increases with increasing C_{NaCl} . We deduce that the polymer chain mobility inside the coacervates upon shear is significantly regulated by ionic strength that promotes the π - π stacking of guanidinium pairs.

3.5. Interaction Force Measurement Using a Surface Force Apparatus. We used a miniature surface force apparatus (μ SFA) to characterize the interaction energy of the guanidinium stacking as a function of C_{NaCl} . Figure 5a,b shows the force–distance profiles between the two symmetric surfaces exposed to salty solutions of $C_{\text{NaCl}} = 0, 0.3, 0.6, 0.9$,

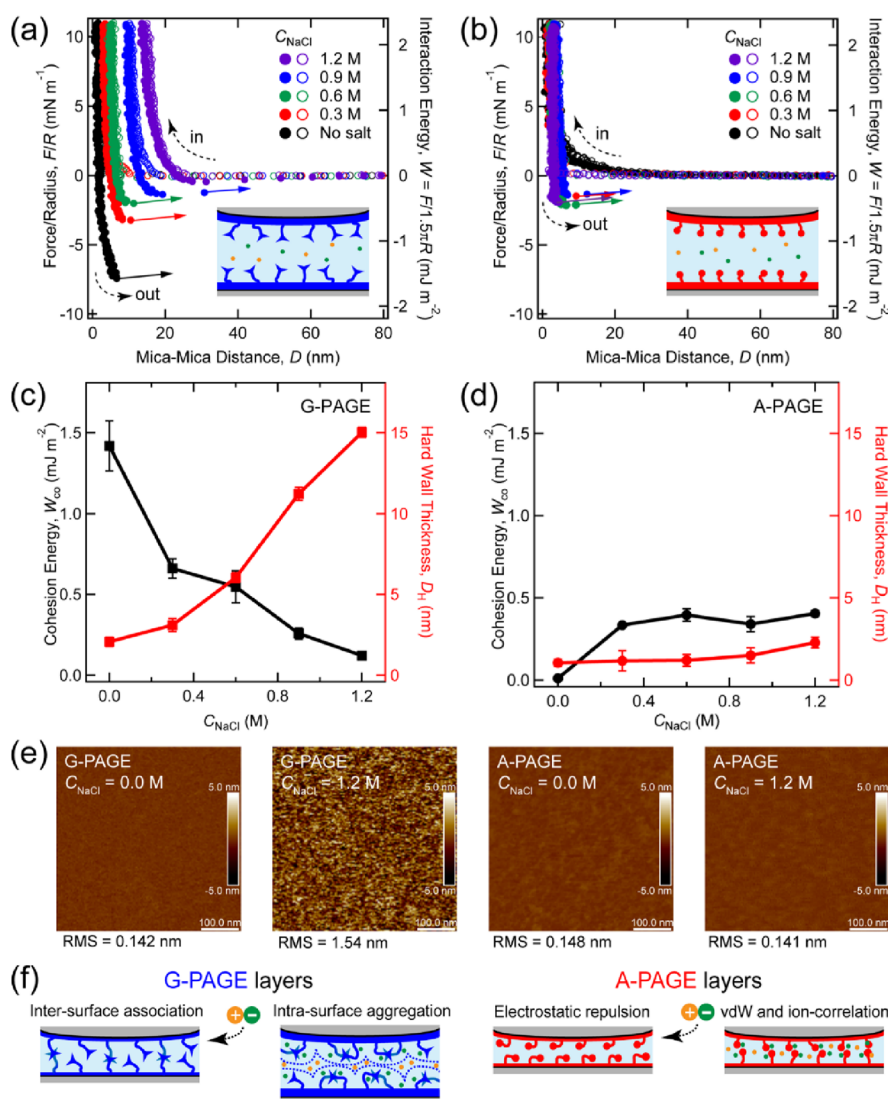


Figure 5. Force–distance profile during approaching and receding of (a) G-PAGE layers and (b) A-PAGE layers in 0 M (black), 0.3 M (red), 0.6 M (green), 0.9 M (blue), and 1.2 M (purple) NaCl solutions. The vacant symbols represent the approaching process, and the filled symbols indicate separation of the two surfaces. Cohesion energy (W_{co} , black) and hard wall distance (D_{H} , red) of (c) G-PAGE and (d) A-PAGE as a function of C_{NaCl} . (e) Surface topography of G-PAGE and A-PAGE layers without salt and with $C_{\text{NaCl}} = 1.2$ M using atomic force microscopy (AFM). (f) Schematic illustration of the G-PAGE and A-PAGE surfaces associated with the salt treatment.

and 1.2 M for G-PAGE and A-PAGE, respectively. The force–distance profiles during moving-in and moving-out of the two surfaces are not overlapped, and this discrepancy, called the adhesion hysteresis, is usually observed for adhesive materials.^{68,69} The approaching force curve represents both the electrostatic repulsion between positively charged surfaces and the steric hindrance of the polymer chains, which provides the hard wall thickness, D_{H} , of the bound polymer layer on the mica surface. The receding force curve measures the attractive interaction between two surfaces, resulting in the cohesion energy per unit area, W_{co} , of the polymer layer. Both W_{co} and D_{H} as a function of C_{NaCl} for G-PAGE and A-PAGE layers are shown in Figure 5c,d, respectively.

A significant adhesion between the two G-PAGE surfaces at $C_{\text{NaCl}} = 0$ M was detected, which stands in contrast to the A-PAGE surfaces where no adhesion was detected at $C_{\text{NaCl}} = 0$ M. This is clear evidence that the π - π stacked guanidinium pair can be formed below a critical salt concentration of coacervation, consistent with the MD results. This further

supports that simple coacervation occurs when the number of guanidinium pairs goes beyond a critical value to create the interchain network formation.

For the G-PAGE layers, W_{co} decreases, and D_{H} significantly increases with increasing C_{NaCl} while both values are nearly independent of C_{NaCl} for the A-PAGE layers. It is interesting that the interfacial behavior of G-PAGE is counterintuitive and looks inconsistent with the bulk properties observed. We further performed atomic force microscopy (AFM) to investigate the surface morphology of A-PAGE and G-PAGE layers as displayed in Figure 5e. As C_{NaCl} increases, the surface roughness becomes more significant for the G-PAGE layer while intact for the A-PAGE layer; root mean square (RMS) values were calculated as 0.142 and 1.54 nm for $C_{\text{NaCl}} = 0$ and 1.2 M, respectively, for the G-PAGE layers. It is reasonable that a large number of guanidinium pairs produce intrasurface aggregates on the mica surface at higher C_{NaCl} , resulting in a rougher and thicker surface of the G-PAGE layers as illustrated in Figure 5f.

As observed in the rheological measurement, chain relaxation in the G-PAGE coacervates requires the dissociation and pair rearrangement of a number of guanidinium stackings. This is a slow process when the activation energy of $\sim 60\text{--}70$ kJ/mol is considered. In addition, for the SFA measurement, the bound chains on the mica surface and a lack of external stimulus such as shear retard the chain relaxation more than bulk coacervates. Therefore, once the intrasurface aggregates are produced, intersurface pairing occurs fairly slowly when two surfaces come into contact. The slow chain dynamics associated with the rough surface lead to the lower probability of forming the intersurface guanidinium pair, resulting in the lower W_{co} at higher C_{NaCl} . It is noted that the force–distance profile is nearly independent of the contact time up to 1 h (data are not shown).

For the A-PAGE layers, a slight increase in W_{co} with increasing C_{NaCl} is attributed to the van der Waals interaction and additional ion-correlation effect when electrostatic repulsion is effectively screened,⁷⁰ which is reasonably consistent with non-attractive polymers. However, associative guanidinium pairing plays a significant role in determining the cohesion property for the G-PAGE layers. Slower chain dynamics due to associative pairing and a high charge density of G-PAGE mainly lead to the observed C_{NaCl} -dependent behavior of W_{co} and D_{H} . This hypothesis suggests that the optimized charge density of the guanidinium group in a polyelectrolyte system opens a window to measure the interaction energy of guanidinium stacking, which suggests a promising future avenue for experiments.

4. CONCLUSIONS

In this work, we demonstrate the simple coacervation of a guanidinium-containing polyelectrolyte triggered by monovalent salts and investigate the phase separation mechanism considering the effect of salt and temperature on the $\pi\text{--}\pi$ interaction. The synthetic route confirms that phase separation is exclusively originated through a face-to-face stacked structure of the cationic guanidinium groups. Although the guanidinium pairs can exist at a lower salt concentration, simple coacervation occurs when the number of guanidinium pairs and, thus, intermolecular interactions goes beyond a critical value to produce the network structure. In particular, the critical temperature monotonically increases with increasing monovalent salt concentration, regardless of the anion type. The strong dependence of the salt concentration and monovalent anion type on the upper critical solution temperature reveals that the associative $\pi\text{--}\pi$ interaction becomes dominant when long-ranged electrostatic repulsion is significantly attenuated, and thus, phase separation can be precisely controlled. Furthermore, the dynamic characteristics of the $\pi\text{--}\pi$ interaction directly affect both the bulk rheological behavior and interfacial property of the simple coacervates. We believe that our findings provide a fundamental understanding of the phase separation mechanism and the dynamical behavior of $\pi\text{--}\pi$ stacked guanidinium pairs associated with coacervate materials for biological and industrial applications and open new avenues to design complex materials in aqueous media with engineered non-covalent interactions.

■ ASSOCIATED CONTENT

Supporting Information

The Supporting Information is available free of charge at <https://pubs.acs.org/doi/10.1021/acs.macromol.2c02346>.

Polymer synthesis and characterizations, supplementary transmittance results and photographs, example of deconvolution for the FTIR spectra, supplementary table for Langmuir-isotherm fitting parameters, shear rate-dependent viscosity, and Arrhenius plots (Figures S1–S7) (PDF)

■ AUTHOR INFORMATION

Corresponding Author

Soo-Hyung Choi – Department of Chemical Engineering, Hongik University, Seoul 04066, Republic of Korea; orcid.org/0000-0002-4078-6285; Email: shchoi@hongik.ac.kr

Authors

Seung-Hwan Oh – Department of Chemical Engineering, Hongik University, Seoul 04066, Republic of Korea; orcid.org/0000-0003-0996-3463

Jinhoon Lee – School of Energy & Chemical Engineering, Ulsan National Institute of Science and Technology (UNIST), Ulsan 44919, Republic of Korea; orcid.org/0000-0002-8608-027X

Minhwan Lee – School of Chemical and Biological Engineering, Seoul National University, Seoul 08826, Republic of Korea; orcid.org/0000-0001-9875-713X

Suulwoo Kim – School of Chemical and Biological Engineering, Seoul National University, Seoul 08826, Republic of Korea

Won Bo Lee – School of Chemical and Biological Engineering, Seoul National University, Seoul 08826, Republic of Korea; orcid.org/0000-0001-7801-083X

Dong Woog Lee – School of Energy & Chemical Engineering, Ulsan National Institute of Science and Technology (UNIST), Ulsan 44919, Republic of Korea; orcid.org/0000-0002-1572-9270

Complete contact information is available at: <https://pubs.acs.org/doi/10.1021/acs.macromol.2c02346>

Author Contributions

The manuscript was written through contributions of all authors. All authors have given approval to the final version of the manuscript.

Notes

The authors declare no competing financial interest.

■ ACKNOWLEDGMENTS

This work was supported by a National Research Foundation (NRF) grant funded by the Korea Government (MSIT) (nos. 2018R1A5A1024127 and 2021R1A2C2011164) and Hongik University Innovation Support Program Fund.

■ REFERENCES

- (1) McCarty, J.; Delaney, K. T.; Danielsen, S. P. O.; Fredrickson, G. H.; Shea, J.-E. Complete Phase Diagram for Liquid–Liquid Phase Separation of Intrinsically Disordered Proteins. *J. Phys. Chem. Lett.* **2019**, *10*, 1644–1652.
- (2) Deepankumar, K.; Guo, Q.; Mohanram, H.; Lim, J.; Mu, Y.; Pervushin, K.; Yu, J.; Miserez, A. Liquid–Liquid Phase Separation of the Green Mussel Adhesive Protein Pvfp-5 is Regulated by the Post-Translated Dopa Amino Acid. *Adv. Mater.* **2022**, *34*, 2103828.
- (3) Kim, S.; Huang, J.; Lee, Y.; Dutta, S.; Yoo, H. Y.; Jung, Y. M.; Jho, Y.; Zeng, H.; Hwang, D. S. Complexation and coacervation of

- like-charged polyelectrolytes inspired by mussels. *Proc. Natl. Acad. Sci. U. S. A.* **2016**, *113*, E847.
- (4) Yeo, G. C.; Keeley, F. W.; Weiss, A. S. Coacervation of tropoelastin. *Adv. Colloid Interface Sci.* **2011**, *167*, 94–103.
- (5) Pak, C. W.; Kosno, M.; Holehouse, A. S.; Padrick, S. B.; Mittal, A.; Ali, R.; Yunus, A. A.; Liu, D. R.; Pappu, R. V.; Rosen, M. K. Sequence Determinants of Intracellular Phase Separation by Complex Coacervation of a Disordered Protein. *Mol. Cell* **2016**, *63*, 72–85.
- (6) Overbeek, J. T. G.; Voorn, M. J. Phase separation in polyelectrolyte solutions. Theory of complex coacervation. *J. Cell. Comp. Physiol.* **1957**, *49*, 7–26.
- (7) Srivastava, S.; Tirrell, M. V. POLYELECTROLYTE COMPLEXATION. *Adv. Chem. Phys.* **2016**, 499–544.
- (8) Lin, Y.-H.; Forman-Kay, J. D.; Chan, H. S. Sequence-Specific Polyampholyte Phase Separation in Membraneless Organelles. *Phys. Rev. Lett.* **2016**, *117*, No. 178101.
- (9) Mitrea, D. M.; Kriwacki, R. W. Phase separation in biology; functional organization of a higher order. *Cell. Commun. Signal.* **2016**, *14*, 1–7.
- (10) Lee, B. P.; Messersmith, P. B.; Israelachvili, J. N.; Waite, J. H. Mussel-Inspired Adhesives and Coatings. *Annu. Rev. Mater. Res.* **2011**, *41*, 99–132.
- (11) Hartl, F. U. Protein Misfolding Diseases. *Annu. Rev. Biochem.* **2017**, *86*, 21–26.
- (12) Wright, P. E.; Dyson, H. J. Intrinsically disordered proteins in cellular signalling and regulation. *Nat. Rev. Mol. Cell Biol.* **2015**, *16*, 18–29.
- (13) Vernon, R. M.; Chong, P. A.; Tsang, B.; Kim, T. H.; Bah, A.; Farber, P.; Lin, H.; Forman-Kay, J. Pi-Pi contacts are an overlooked protein feature relevant to phase separation. *eLife* **2018**, *7*, No. e31486.
- (14) Kubičková, A.; Křížek, T.; Coufal, P.; Wernersson, E.; Heyda, J.; Jungwirth, P. Guanidinium Cations Pair with Positively Charged Arginine Side Chains in Water. *J. Phys. Chem. Lett.* **2011**, *2*, 1387–1389.
- (15) Shih, O.; England, A. H.; Dallinger, G. C.; Smith, J. W.; Duffey, K. C.; Cohen, R. C.; Prendergast, D.; Saykally, R. J. Cation-cation contact pairing in water: Guanidinium. *J. Chem. Phys.* **2013**, *139*, No. 035104.
- (16) Heiles, S.; Cooper, R. J.; DiTucci, M. J.; Williams, E. R. Hydration of guanidinium depends on its local environment. *Chem. Sci.* **2015**, *6*, 3420–3429.
- (17) Mason, P. E.; Neilson, G. W.; Enderby, J. E.; Saboungi, M.; Dempsey, C. E.; MacKerell, A. D.; Brady, J. W. The Structure of Aqueous Guanidinium Chloride Solutions. *J. Am. Chem. Soc.* **2004**, *126*, 11462–11470.
- (18) Mason, P. E.; Brady, J. W.; Neilson, G. W.; Dempsey, C. E. The interaction of guanidinium ions with a model peptide. *Biophys. J.* **2007**, *93*, L04–L06.
- (19) McKinlay, C. J.; Waymouth, R. M.; Wender, P. A. Cell-Penetrating, Guanidinium-Rich Oligophosphoesters: Effective and Versatile Molecular Transporters for Drug and Probe Delivery. *J. Am. Chem. Soc.* **2016**, *138*, 3510–3517.
- (20) Tesei, G.; Vazdar, M.; Jensen, M. R.; Cragnell, C.; Mason, P. E.; Heyda, J.; Skepö, M.; Jungwirth, P.; Lund, M. Self-association of a highly charged arginine-rich cell-penetrating peptide. *Proc. Natl. Acad. Sci. U. S. A.* **2017**, *114*, 11428.
- (21) Vazdar, M.; Heyda, J.; Mason, P. E.; Tesei, G.; Allolio, C.; Lund, M.; Jungwirth, P. Arginine “Magic.” Guanidinium Like-Charge Ion Pairing from Aqueous Salts to Cell Penetrating Peptides. *Acc. Chem. Res.* **2018**, *51*, 1455–1464.
- (22) Kim, H.; Jeon, B. J.; Kim, S.; Jho, Y.; Hwang, D. S. Upper Critical Solution Temperature (UCST) Behavior of Coacervate of Cationic Protamine and Multivalent Anions. *Polymers* **2019**, *11*, 691.
- (23) Prather, L. J.; Weerasekare, G. M.; Sima, M.; Quinn, C.; Stewart, R. J. Aqueous Liquid-Liquid Phase Separation of Natural and Synthetic Polyguanidiniums. *Polymers* **2019**, *11*, 649.
- (24) Yang, B.; Jin, S.; Park, Y.; Jung, Y. M.; Cha, H. J. Coacervation of Interfacial Adhesive Proteins for Initial Mussel Adhesion to a Wet Surface. *Small* **2018**, *14*, 1803377.
- (25) Zydziak, N.; Iqbal, M. H.; Chaumont, A.; Combes, A.; Wasielewski, E.; Legros, M.; Jierry, L.; Lavalle, P.; Boulmedais, F.; Chan-Seng, D. Unexpected aqueous UCST behavior of a cationic comb polymer with pentaarginine side chains. *Eur. Polym. J.* **2020**, *125*, No. 109528.
- (26) Kim, S.; Lee, M.; Lee, W. B.; Choi, S.-H. Ionic-Group Dependence of Polyelectrolyte Coacervate Phase Behavior. *Macromolecules* **2021**, *54*, 7572–7581.
- (27) Neitzel, A. E.; Fang, Y. N.; Yu, B.; Rumyantsev, A. M.; de Pablo, J. J.; Tirrell, M. V. Polyelectrolyte Complex Coacervation across a Broad Range of Charge Densities. *Macromolecules* **2021**, *54*, 6878–6890.
- (28) Wong, L. E.; Kim, T. H.; Muhandiram, D. R.; Forman-Kay, J. D.; Kay, L. E. NMR Experiments for Studies of Dilute and Condensed Protein Phases: Application to the Phase-Separating Protein CAPRIN1. *J. Am. Chem. Soc.* **2020**, *142*, 2471–2489.
- (29) Ferrari, L.; Stucchi, R.; Konstantoulea, K.; van de Kamp, G.; Kos, R.; Geerts, W. J. C.; van Bezouwen, L. S.; Förster, F. G.; Altelaar, M.; Hoogenraad, C. C.; Rüdiger, S. G. D. Arginine π -stacking drives binding to fibrils of the Alzheimer protein Tau. *Nat. Commun.* **2020**, *11*, 571.
- (30) Lee, B. F.; Kade, M. J.; Chute, J. A.; Gupta, N.; Campos, L. M.; Fredrickson, G. H.; Kramer, E. J.; Lynd, N. A.; Hawker, C. J. Poly(allyl glycidyl ether)-A versatile and functional polyether platform. *J. Polym. Sci., Part A: Polym. Chem.* **2011**, *49*, 4498–4504.
- (31) Kade, M. J.; Burke, D. J.; Hawker, C. J. The power of thiol-ene chemistry. *J. Polym. Sci., Part A: Polym. Chem.* **2010**, *48*, 743–750.
- (32) Bernatowicz, M. S.; Wu, Y.; Matsueda, G. R. 1H-Pyrazole-1-carboxamide hydrochloride an attractive reagent for guanylation of amines and its application to peptide synthesis. *J. Org. Chem.* **1992**, *57*, 2497–2502.
- (33) Berendsen, H. J. C.; van der Spoel, D.; van Drunen, R. GROMACS: a message-passing parallel molecular dynamics implementation. *Comput. Phys. Commun.* **1995**, *91*, 43–56.
- (34) Lindahl, E.; Hess, B.; Van Der Spoel, D. GROMACS 3.0: a package for molecular simulation and trajectory analysis. *Mol. Model. Annu.* **2001**, *7*, 306–317.
- (35) Van Der Spoel, D.; Lindahl, E.; Hess, B.; Groenhof, G.; Mark, A. E.; Berendsen, H. J. C. GROMACS: fast, flexible, and free. *J. Comput. Chem.* **2005**, *26*, 1701–1718.
- (36) Jorgensen, W. L.; Maxwell, D. S.; Tirado-Rives, J. Development and testing of the OPLS all-atom force field on conformational energetics and properties of organic liquids. *J. Am. Chem. Soc.* **1996**, *118*, 11225–11236.
- (37) Jorgensen, W. L.; Tirado-Rives, J. Potential energy functions for atomic-level simulations of water and organic and biomolecular systems. *Proceedings of the National Academy of Sciences* **2005**, *102*, 6665–6670.
- (38) Dodda, L. S.; Vilseck, J. Z.; Tirado-Rives, J.; Jorgensen, W. L. 1.14* CM1A-LBCC: localized bond-charge corrected CM1A charges for condensed-phase simulations. *The Journal of Physical Chemistry B* **2017**, *121*, 3864–3870.
- (39) Dodda, L. S.; Cabeza de Vaca, I.; Tirado-Rives, J.; Jorgensen, W. L. LigParGen web server: an automatic OPLS-AA parameter generator for organic ligands. *Nucleic Acids Res.* **2017**, *45*, W331–W336.
- (40) Darden, T.; York, D.; Pedersen, L. Particle mesh Ewald: An $N \cdot \log(N)$ method for Ewald sums in large systems. *J. Chem. Phys.* **1993**, *98*, 10089–10092.
- (41) Bussi, G.; Donadio, D.; Parrinello, M. Canonical sampling through velocity rescaling. *J. Chem. Phys.* **2007**, *126*, No. 014101.
- (42) Berendsen, H. J. C.; Postma, J. P. M.; van Gunsteren, W. F.; DiNola, A.; Haak, J. R. Molecular dynamics with coupling to an external bath. *J. Chem. Phys.* **1984**, *81*, 3684–3690.
- (43) Nosé, S. A unified formulation of the constant temperature molecular dynamics methods. *J. Chem. Phys.* **1984**, *81*, 511–519.

- (44) Hoover, W. G. Canonical dynamics: Equilibrium phase-space distributions. *Phys. Rev. A* **1985**, *31*, 1695.
- (45) Parrinello, M.; Rahman, A. Polymorphic transitions in single crystals: A new molecular dynamics method. *J. Appl. Phys.* **1981**, *52*, 7182–7190.
- (46) Nosé, S.; Klein, M. L. Constant pressure molecular dynamics for molecular systems. *Mol. Phys.* **1983**, *50*, 1055–1076.
- (47) Israelachvili, J.; Min, Y.; Akbulut, M.; Alig, A.; Carver, G.; Greene, W.; Kristiansen, K.; Meyer, E.; Pesika, N.; Rosenberg, K.; Zeng, H. Recent advances in the surface forces apparatus (SFA) technique. *Rep. Prog. Phys.* **2010**, *73*, No. 036601.
- (48) Kristiansen, K.; Donaldson, S. H.; Berkson, Z. J.; Scott, J.; Su, R.; Banquy, X.; Lee, D. W.; de Aguiar, H. B.; McGraw, J. D.; Degen, G. D.; Israelachvili, J. N. Multimodal Miniature Surface Forces Apparatus (μ SFA) for Interfacial Science Measurements. *Langmuir* **2019**, *35*, 15500–15514.
- (49) Israelachvili, J. N. Thin film studies using multiple-beam interferometry. *J. Colloid Interface Sci.* **1973**, *44*, 259–272.
- (50) Johnson, K. L.; Kendall, K.; Roberts, A. D.; Tabor, D. Surface energy and the contact of elastic solids. *Proc. R. Soc. London, Ser. A* **1971**, *324*, 301–313.
- (51) Vorobyev, D. Y.; Kuo, C.; Kuroda, D. G.; Scott, J. N.; Vanderkooi, J. M.; Hochstrasser, R. M. Water-Induced Relaxation of a Degenerate Vibration of Guanidinium Using 2D IR Echo Spectroscopy. *J. Phys. Chem. B* **2010**, *114*, 2944–2953.
- (52) Ghosh, A.; Tucker, M. J.; Hochstrasser, R. M. Identification of Arginine Residues in Peptides by 2D-IR Echo Spectroscopy. *J. Phys. Chem. A* **2011**, *115*, 9731–9738.
- (53) Chirgadze, Y. N.; Fedorov, O. V.; Trushina, N. P. Estimation of amino acid residue side-chain absorption in the infrared spectra of protein solutions in heavy water. *Biopolymers* **1975**, *14*, 679–694.
- (54) Batty, C. J.; Hoath, S. D.; Roberts, B. L. Measurement of Lorentzian linewidths: Numerical evaluation of the Voigt integral. *Nucl. Instrum. Methods* **1976**, *137*, 179–181.
- (55) Vondrášek, J.; Mason, P. E.; Heyda, J.; Collins, K. D.; Jungwirth, P. The Molecular Origin of Like-Charge Arginine–Arginine Pairing in Water. *J. Phys. Chem. B* **2009**, *113*, 9041–9045.
- (56) Schwierz, N.; Horinek, D.; Sivan, U.; Netz, R. R. Reversed Hofmeister series—The rule rather than the exception. *Curr. Opin. Colloid Interface Sci.* **2016**, *23*, 10–18.
- (57) Marcus, Y. Thermodynamics of solvation of ions. Part 5.—Gibbs free energy of hydration at 298.15 K. *J. Chem. Soc., Faraday Trans* **1991**, *87*, 2995–2999.
- (58) Zhang, Y.; Cremer, P. S. The inverse and direct Hofmeister series for lysozyme. *Proc. Natl. Acad. Sci. U. S. A.* **2009**, *106*, 15249–15253.
- (59) Zhang, Y.; Furyk, S.; Bergbreiter, D. E.; Cremer, P. S. Specific Ion Effects on the Water Solubility of Macromolecules: PNIPAM and the Hofmeister Series. *J. Am. Chem. Soc.* **2005**, *127*, 14505–14510.
- (60) Rubinstein, M.; Semenov, A. N. Dynamics of Entangled Solutions of Associating Polymers. *Macromolecules* **2001**, *34*, 1058–1068.
- (61) Zhang, Z.; Chen, Q.; Colby, R. H. Dynamics of associative polymers. *Soft Matter* **2018**, *14*, 2961–2977.
- (62) Marx, V. Cell biology befriends soft matter physics. *Nat. Methods* **2020**, *17*, 567–570.
- (63) Martin Erik, W.; Holehouse Alex, S.; Ivan, P.; Mina, F.; Jeremias, I. J.; Anne, B.; Grace Christy, R.; Andrea, S.; Pappu Rohit, V.; Tanja, M. Valence and patterning of aromatic residues determine the phase behavior of prion-like domains. *Science* **2020**, *367*, 694–699.
- (64) Semenov, A. N.; Rubinstein, M. Dynamics of Entangled Associating Polymers with Large Aggregates. *Macromolecules* **2002**, *35*, 4821–4837.
- (65) Hamad, F. G.; Chen, Q.; Colby, R. H. Linear Viscoelasticity and Swelling of Polyelectrolyte Complex Coacervates. *Macromolecules* **2018**, *51*, 5547–5555.
- (66) No, K. T.; Nam, K.-Y.; Scheraga, H. A. Stability of Like and Oppositely Charged Organic Ion Pairs in Aqueous Solution. *J. Am. Chem. Soc.* **1997**, *119*, 12917–12922.
- (67) Masunov, A.; Lazaridis, T. Potentials of Mean Force between Ionizable Amino Acid Side Chains in Water. *J. Am. Chem. Soc.* **2003**, *125*, 1722–1730.
- (68) Chen, Y. L.; Helm, C. A.; Israelachvili, J. N. Molecular mechanisms associated with adhesion and contact angle hysteresis of monolayer surfaces. *J. Phys. Chem.* **1991**, *95*, 10736–10747.
- (69) Chaudhury, M. K.; Owen, M. J. Adhesion hysteresis and friction. *Langmuir* **1993**, *9*, 29–31.
- (70) Guldbrand, L.; Jönsson, B.; Wennerström, H.; Linse, P. Electrical double layer forces. A Monte Carlo study. *J. Chem. Phys.* **1984**, *80*, 2221–2228.